Proc. Natl. Acad. Sci. USA
Vol. 92, pp. 9490–9494, October 1995
Medical Sciences

Tertiary structure of an amyloid immunoglobulin light chain protein: A proposed model for amyloid fibril formation

(x-ray crystallography/amyloid light chain amyloidosis)

NORBERT SCHORMANN*, JILL R. MURRELL*, JURIS J. LIEPNIEKS†, AND MERRILL D. BENSON*†‡

Departments of *Medicine and ‡Medical and Molecular Genetics, Indiana University School of Medicine, Indianapolis, IN 46202; and the †Richard L. Roudebush Veterans Affairs Medical Center, Indianapolis, IN 46202

Communicated by Frank W. Putnam, Indiana University, Bloomington, IN, June 22, 1995

ABSTRACT **An immunoglobulin light chain protein was isolated from the urine of an individual (BRE) with systemic amyloidosis. Complete amino acid sequence of the variable region of the light chain (V_L) protein established it as a κ I, which when compared with other κ I amyloid associated proteins had unique residues, including Ile-34, Leu-40, and Tyr-71. To study the tertiary structure, BRE V_L was expressed in *Escherichia coli* by using a PCR product amplified from the patient BRE's bone marrow DNA. The PCR product was ligated into pCZ11, a thermal-inducible replication vector. Recombinant BRE V_L was isolated, purified to homogeneity, and crystallized by using ammonium sulfate as the precipitant. Two crystal forms were obtained. In crystal form I the BRE V_L κ domain crystallizes as a dimer with unit cell constants isomorphous to previously published κ protein structures. Comparison with a nonamyloid V_L κ domain from patient REI, identified significant differences in position of residues in the hypervariable segments plus variations in framework region (FR) segments 40–46 (FR2) and 66–67 (FR3). In addition, positional differences can be seen along the two types of local diads, corresponding to the monomer–monomer and dimer–dimer interfaces. From the packing diagram, a model for the amyloid light chain (AL) fibril is proposed based on a pseudohexagonal spiral structure with a rise of approximately the width of two dimers per 360° turn. This spiral structure could be consistent with the dimensions of amyloid fibrils as determined by electron microscopy.**

Immunocyte-derived amyloid light chain (AL) (primary) amyloidosis is the most common form of systemic amyloidosis and, of all the amyloidoses, is associated with the shortest survival rate (1). In the majority of cases, this disease is associated with a nonmalignant expansion of a single plasma cell clone. It is the monoclonal immunoglobulin light chain product of the plasma cell clone which is the precursor of the amyloid fibril subunit protein (2).

A number of clinically observed features of AL amyloidosis suggest that structure of the immunoglobulin light chain subunit protein is an important factor in the pathogenesis of this disease. First, while the ratio of κ to λ plasma cell clones and proteins in the human is 3:2, more individuals with λ light chain-derived amyloid are identified than with κ proteins. Second, within the λ light chain subgroups, the λ VI proteins have been found to be particularly amyloidogenic (3, 4). Third, κ I light chain proteins represent the majority of κ amyloid proteins and primary structure analyses have suggested substitutions in key framework regions as being associated with amyloid fibril formation (5) (see Fig. 1).

To investigate structural factors which may be important for amyloid fibril formation from immunoglobulin light chain proteins, an attempt has been made to compare the structure of the variable region of an amyloid light chain protein with the structure of nonamyloid light chain proteins. The goal is to develop a structural model for the polymerization or aggregation process of immunoglobulin light chain proteins which leads to amyloid fibril formation. A κ I protein from an individual with amyloidosis was completely characterized at the primary structure level.

By using the determined amino acid sequence, oligonucleotide primers were constructed and used to amplify from the patient's bone marrow DNA the sequence coding for the entire variable segment of the κ I light chain.§ The DNA construct was then used to express the recombinant variable region of the light chain (V_L) of the κ I protein *in vitro*. This protein was crystallized, and its tertiary structure was determined by x-ray diffraction.¶

MATERIALS AND METHODS

Isolation and Characterization of Light Chain Protein BRE. Light chain protein was isolated from the urine of patient BRE (hereafter referred to as BRE protein or BRE) by precipitation in 60% ammonium sulfate followed by chromatography on DEAE cellulose and ACA-34 (Pharmacia). Amino acid sequence analysis was performed on a Beckman 890C sequenator as described (4). For a complete structure, the BRE protein was digested with L-1-tosylamido-2-phenylethyl chloromethyl ketone (TPCK)-treated trypsin and resultant peptides separated on a C_{18} HPLC column.

DNA Isolation and Plasmid Construction for Expression of Recombinant Protein. DNA was isolated from bone marrow cells of patient BRE by using the method of Madisen *et al.* (6). On the basis of the amino acid sequence of BRE protein and published sequences of the signal peptide for κ I proteins (7), oligonucleotide primers were constructed (see Fig. 2). The resultant PCR amplification product was then ligated into pCZ11, a thermoinducible replication vector, and used to transform competent *Escherichia coli* strain HB101 (8). As described for transthyretin (TTR) (8), cell pellets of positive HB101 pCZ11/BRE clones grown in culture were subjected to SDS/12.5% PAGE. Electrophoresed proteins were transferred to polyvinylidene difluoride (PVDF) membrane (Applied Biosystems) and subjected to (*i*) Western analysis using BRE-specific antiserum and (*ii*) amino acid sequencing of bands of appropriate molecular weight (ABI 473A sequenator; Applied Biosystems).

The publication costs of this article were defrayed in part by page charge payment. This article must therefore be hereby marked "*advertisement*" in accordance with 18 U.S.C. §1734 solely to indicate this fact.

Abbreviations: V_L, variable region of the light chain; FR, framework region; CDR, complementarity-determining region; AL, amyloid light chain.

§The sequence reported in this paper has been deposited in the GenBank data base (accession no. U31344).

¶The atomic coordinates and structure factors have been deposited in the Protein Data Bank, Chemistry Department, Brookhaven National Laboratory, Upton, NY, 11973 (references 1BRE and R1BRESF).

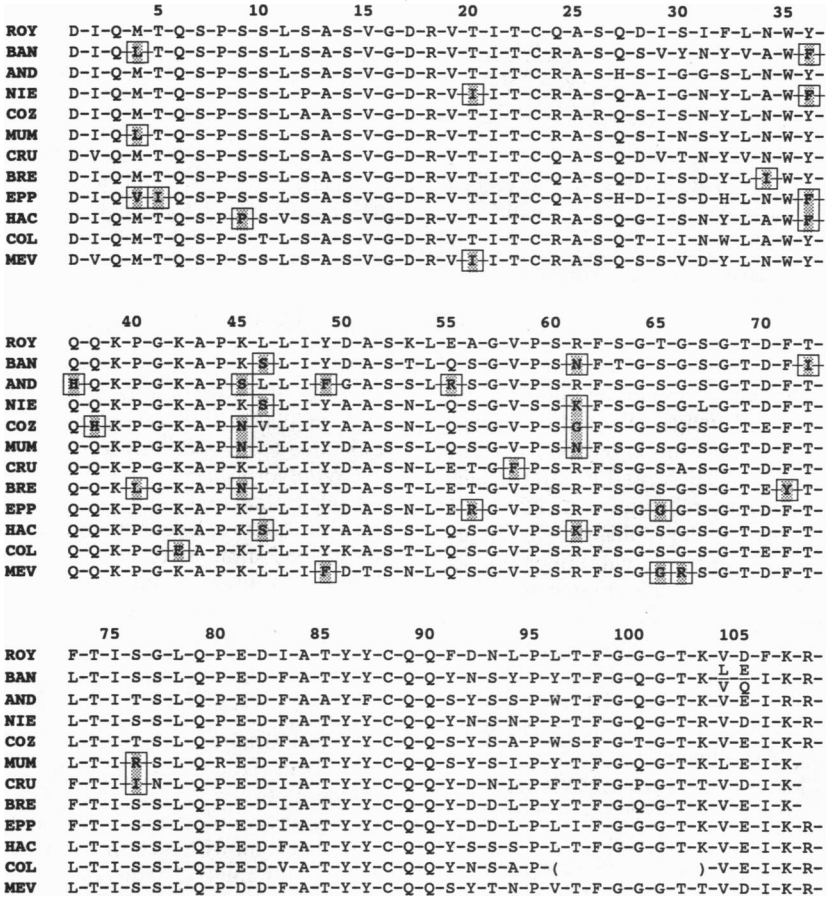

FIG. 1. Complete V_L amino acid sequences for known κ I amyloid proteins compared with a non-amyloid myeloma protein (ROY). ROY sequence is taken from ref. 7, and MEV sequence is taken from ref. 20. BAN and MUM both have N-linked carbohydrate on residue 61. Residues of amyloid proteins possibly associated with fibril formation are boxed and shaded (5).

Large Scale Growth and Protein Isolation. Cells containing the desired plasmid were grown in 200 ml of TY broth (0.8% tryptone/1% yeast extract/0.25% NaCl) overnight at 23°C as described (8). This culture was added to 4.5 l of TY broth in a 5-l Bioflo III Bioreactor (New Brunswick Scientific), and grown at 40°C with monitoring of O_2 saturation and pH. After 6 h, the culture was centrifuged, and the cell pellet was isolated and lysed by freeze/thaw and sonication. The supernatant was fractionated by DEAE cellulose, and fractions containing protein BRE were then subjected to further purification on ACA-34.

Crystallization and X-Ray Analysis. Purified protein BRE was concentrated to 20 mg/ml in 0.1 M Tris buffer, pH 7.5. Crystals of BRE with a size of 0.35 × 0.3 × 0.25 mm were grown by hanging-drop vapor diffusion against 2.25–2.5 M ammonium sulfate in 100 mM citrate buffer, pH 5.5, at 23°C. Two crystal forms were obtained under very similar conditions. Crystal form I belongs to the monoclinic system, space group $P2_1$, with unit-cell dimensions of a = 82.29 Å, b = 77.73 Å, c = 82.20 Å, and β = 119.95° ($V \approx 450{,}000$ Å^3) and six monomers (6 × 12 kDa) in the asymmetric unit. These unit-cell constants are isomorphous to those published for κ ROY (9); however, the κ BRE intensities do not exhibit hexagonal symmetry. Crystal form II, on the other hand, belongs to the orthorhombic space group $C222_1$, with unit-cell dimensions of a = 82.04 Å, b = 142.09 Å, and c = 77.85 Å ($V \approx 900{,}000$ Å^3) and three monomers in the asymmetric unit.

All data were collected on an R-Axis IIC image plate area detector (Molecular Structure, The Woodlands, TX) by using a Rigaku RU-200 x-ray source and were reduced with R-Axis processing software (10).

Structure Determination. *Crystal form I (BRE I).* A native data set was collected on a single crystal to a nominal resolution of 1.75 Å (see Table 1). Molecular replacement (rotation and translation searches together with Patterson correlation refinement) was performed with X-PLOR (11, 12) by using data in the 15- to 3.5-Å shell and the refined REI structure as the search model (13). Each independent solution from the cross-rotation function after PC refinement (11) was used in a translation search in the a and c directions since this space group requires only a search in x and z. The best solution for the first translation function gave the position of dimer 1 in the asymmetric unit. To determine the relative position of dimer 2 and 3 with respect to dimer 1, we used combined translation functions (11). A rough overall model with appropriate amino acid substitutions made by using QUANTA [QUANTA 4.0 (1994); Molecular Modeling Software Package, Polygen Corp., Waltham, MA] was then submitted to rigid body and Powell minimization refinement with X-PLOR (12). After subsequent refinement using a simulated annealing protocol in

Table 1. Statistics of x-ray data collection for BRE

	BRE I	BRE II
Resolution range, Å	71.19–1.75	52.45–1.75
Number of unique reflections	42,843	27,515
% completeness of data	77.3 (2.5 Å)	85.0 (2.5 Å)
(resolution limit, Å)	57.0 (2.0 Å)	72.8 (2.0 Å)
	47.1 (1.75 Å)	59.5 (1.75 Å)
R_{merge}, %*	10.12	7.55

*$R_{merge} = \Sigma_i |\langle I \rangle - I_i| / \Sigma_i I_i$; R_{merge} (all reflections) was calculated for the observations with $I > \sigma$ (I).

Table 2. Refinement statistics of BRE I

	X-PLOR*	PROLSQ*	X-PLOR†	PROLSQ†
Resolution range, Å	5.0–2.0	5.0–2.0	5.0–2.0	5.0–2.0
Refinement *R* factor, %‡	21.8	19.3	23.7	19.8
Number of protein atoms	4974	4974	4974	4974
Number of water molecules	54	60	45	40
Average *B* factors for protein atoms, Å^2	16.83	11.04	15.89	8.74
rms bond length deviation, Å	0.013	0.023 (σ = 0.025)	0.015	0.021 (σ = 0.02)
rms bond angle deviation,°	2.1	3.5	1.9	4.3

*Without noncrystallographic symmetry restraints.
†With noncrystallographic symmetry restraints.
‡$R = \Sigma_{hkl}\,(||F_{obs_{hkl}}| - |F_{calc_{hkl}}||/|F_{obs_{hkl}}|)$, where $|F_{obs_{hkl}}|$ and $|F_{calc_{hkl}}|$, are the observed and calculated structure factor amplitudes.

X-PLOR (14) with intermittent cycles of model rebuilding using O (15) by inspection of $2F_o - F_c$ maps, all residues except Arg-108 in each monomer were clearly observed. Refinement was carried out to a resolution of 2.0 Å, and in later stages water molecules found by a peak search routine in CCP4 (16) were gradually added. No noncrystallographic symmetry restraints were used at this point. After positional refinement, as implemented in X-PLOR (12), the crystallographic *R* factor dropped to 21.8% for all data in the resolution range 5.0–2.0 Å. To assess the quality of the refinement, we used the free *R*-factor test in X-PLOR (17). The high value ($R_{free} \approx 33.7\%$) indicated possible overfitting of our model. To improve the data-to-parameter ratio, we included noncrystallographic symmetry restraints and repeated the refinement with X-PLOR (12, 14). The crystallographic *R* factor converged at 22.9% ($R_{free} \approx$ 26%). Finally, we subjected the model to 10 cycles of restrained least-squares refinement by using PROLSQ (18). The current model consists of 4974 protein atoms (107 of the 108 residues modeled) and 40 water molecules (see Table 2). The present *R* factor is 19.8% (data in resolution range of 5.0–2.0 Å) with an R_{free} of 20.4% (5% of data). The mean coordinate error is estimated to be 0.33 Å by using the SIGMAA method (19).

Crystal form II (BRE II). A native data set was collected on a single crystal to the same nominal resolution of 1.75 Å (Table 1). Molecular replacement with X-PLOR (11) using three of the six refined monomers of crystal form I as a search model reveals a solution which is consistent with our present model showing a very similar packing arrangement. Refinement of this structure is in progress.

RESULTS AND DISCUSSION

Sequence analysis of intact protein BRE isolated from the urine of a patient with systemic amyloidosis identified it as belonging to the κ I subgroup. The complete sequence of its V_L region was determined by analysis of peptides obtained after digestion with trypsin. Comparison of BRE V_L sequence to other κ I amyloid associated proteins showed a few unique residues, including Ile-34, Leu-40, and Tyr-71 (Fig. 1).

By using oligonucleotide primers based on the amino acid sequence of BRE V_L and published κ I signal peptides, PCR amplification of bone marrow DNA from patient BRE gave a product of expected size which by direct sequencing was shown to have nucleotide sequence in agreement with the protein structure of BRE V_L (Fig. 2). Ligation of this DNA construct into pCZ11 and expression in *E. coli* produced a protein of approximately 12,000 Da. This protein reacted specifically with an antiserum raised against the BRE urine light chain. Recombinant BRE protein was purified to homogeneity and crystallized by using ammonium sulfate as precipitant. Diffraction data to 1.75-Å resolution were collected in two crystal forms (Table 1). The structure of the BRE V_L κ domain in crystal form I was determined by x-ray diffraction and refined to 2 Å (Table 2).

5′ PRIMER

AGA	TGT	GAT	ATC	CAG	ATG	AC			
-2	-1	1	2	3	4	5	6	7	8
ARG	CYS	ASP	ILE	GLN	MET	THR	GLN	SER	PRO
AGA	TGT	GAT	ATC	CAG	ATG	ACG	CAG	TCT	CCA
9	10	11	12	13	14	15	16	17	18
SER	SER	LEU	SER	ALA	SER	VAL	GLY	ASP	ARG
TCC	TCC	CTG	TCT	GCA	TCT	GTA	GGA	GAC	AGA
19	20	21	22	23	24	25	26	27	28
VAL	THR	ILE	THR	CYS	GLN	ALA	SER	GLN	ASP
GTC	ACC	ATC	ACT	TGC	CAG	GCG	AGT	CAG	GAC
29	30	31	32	33	34	35	36	37	38
ILE	SER	ASP	TYR	LEU	ILE	TRP	TYR	GLN	GLN
ATT	AGC	GAC	TAT	TTA	ATT	TGG	TAT	CAG	CAG
39	40	41	42	43	44	45	46	47	48
LYS	LEU	GLY	LYS	ALA	PRO	ASN	LEU	LEU	ILE
AAA	CTA	GGA	AAA	GCC	CCT	AAC	CTC	CTG	ATC
49	50	51	52	53	54	55	56	57	58
TYR	ASP	ALA	SER	THR	LEU	GLU	THR	GLY	VAL
TAC	GAT	GCA	TCC	ACT	TTG	GAA	ACA	GGG	GTC
59	60	61	62	63	64	65	66	67	68
PRO	SER	ARG	PHE	SER	GLY	SER	GLY	SER	GLY
CCA	TCA	AGG	TTC	AGT	GGA	AGT	GGA	TCT	GGC
69	70	71	72	73	74	75	76	77	78
THR	GLU	TYR	THR	PHE	THR	ILE	SER	SER	LEU
ACA	GAG	TAT	ACT	TTC	ACC	ATC	AGC	AGC	CTG
79	80	81	82	83	84	85	86	87	88
GLN	PRO	GLU	ASP	ILE	ALA	THR	TYR	TYR	CYS
CAG	CCT	GAA	GAT	ATT	GCA	ACA	TAT	TAC	TGT
89	90	91	92	93	94	95	96	97	98
GLN	GLN	TYR	ASP	ASP	LEU	PRO	TYR	THR	PHE
CAA	CAA	TAT	GAT	GAT	CTC	CCC	TAC	ACT	TTT
99	100	101	102	103	104	105	106	107	108
GLY	GLN	GLY	THR	LYS	VAL	GLU	ILE	LYS	ARG
GGC	CAG	GGG	ACC	AAG	GTG	GAA	ATC	AAA	CGA

TTC CAC CTT TAG TTT GCT
3′ PRIMER

FIG. 2. Oligonucleotide sequence coding for BRE V_L determined from PCR amplification of bone marrow DNA. The 5′ and 3′ amplification primers were synthesized on the basis of published κ I signal and J_1 joining region sequences.

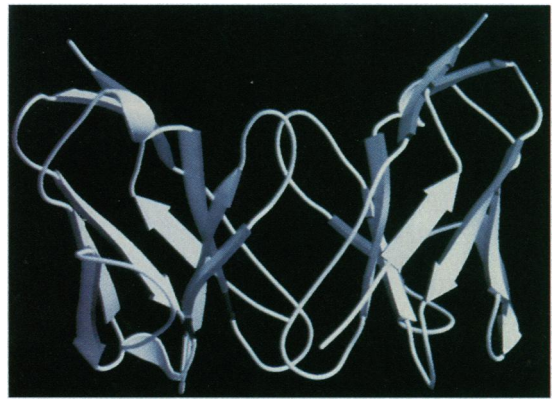

FIG. 3. Ribbon diagram of V_L dimer based on the refined BRE structure. The figure was prepared with MOLSCRIPT (21) and rendered with RASTER3D (22, 23) on the basis of secondary structure assignments made by DSSP (24).

	CDR1			FR2			CDR2				FR3	CDR3		FR4		
Position	30	31	34	39	40	45	50	53	55	56	70	92	93	104	105	107
BRE	SER	ASP	ILE	LYS	LEU	ASN	ASP	THR	GLU	THR	GLU	ASP	ASP	VAL	GLU	LYS
REI	ILE	LYS	ASN	THR	PRO	LYS	GLU	ASN	GLN	ALA	ASP	GLN	SER	LEU	GLN	THR

FIG. 4. Comparison of altered residues in the sequences of BRE and REI and their locations in FRs and CDRs according to Kabat *et al.* (7).

The BRE V_L κ domain crystallizes as a dimer, as found for proteins ROY and REI (9, 13). The tertiary structure of BRE is similar to other λ and κ light chain fragments in that the monomer is composed of a β-barrel formed from nine antiparallel β-strands arranged in two sheets packed against each other, with two monomers making a Bence Jones-type dimer (Fig. 3). Two forms of interdomain contacts can be seen along the two types of local diads. Amino acid residues Tyr-36, Glu-38, Pro-44, Asn-45, Tyr-87, and Phe-98 of both monomers participate in the monomer–monomer contact region, as described for REI (13). The contact region between the noncovalent dimers is formed by amino acid residues Ser-9, Ser-10, and Ser-12 extending the hydrogen bonding network and by Pro-8 and Leu-11 making hydrophobic contacts.

Sequence comparison of BRE with REI shows the altered residues and their assignment to FRs and complementarity-determining regions (CDRs) (Fig. 4). Comparison with the published tertiary structure of REI (13) was accomplished by superimposition of the structures by using a least-squares procedure. Significant differences in the position of residues in the hypervariable segments (residues 28–32, 50–53, and 91–96), as well as variations in FR segments 40–46 (FR2) and 66–67 (FR3), are seen. The largest difference between BRE and REI monomers is in the 40–44 loop which forms part of the dimer interface, partly due to a substitution of Leu for Pro at residue 40. This substitution also introduces a hydrophobic residue into a hydrophilic environment since residue 40 is exposed to the solvent. Important positional differences of residues involved in monomer–monomer interactions at the dimer interface and in monomer–monomer interactions along the dimer–dimer contact region are seen (Fig. 5 *A* and *B*). While topology and hydrogen-bonding pattern of the monomers and interactions overall between monomers at the dimer interface are preserved, there are perturbations in contacts along the dimer–dimer interface. Due to moving apart from each other, the hydrogen bond between the hydroxyl of Ser-10 and the nitrogen of Ser-212 is deleted in BRE, which should result in a destabilization of dimer–dimer contacts.

Proposed Model for the AL Amyloid Fibril. The study of tertiary structure of κ BRE, an amyloid-forming light chain protein, has resulted in the formation of a model of V_L dimers in a pseudohexagonal arrangement with a diameter of 115 Å and a rise of 38.8 Å per turn of 180° (Fig. 6). This would allow a structure that can be visualized as a spiral with six light chain dimers and a rise of approximately the diameter of two dimers per turn of 360° (Fig. 7). This model fits well with the dimensions noted by electron microscopy for fibrils of approximately 10 nm (100 Å) in diameter and indeterminate length.

As for TTR, structural alterations are found in immunoglobulin protein(s) associated with amyloidosis when compared with their nonamyloid counterparts. These changes usually involve residues at the interface (monomer–monomer and dimer–dimer interactions). Both light chain proteins and TTR variants show an extensive β-sheet framework believed to be a prerequisite for fibril formation. In TTR variants, single-site substitutions lead to structural perturbations, but so far all variants studied crystallographically crystallize isomorphously (same space group, very similar unit-cell parameters)—i.e., their packing mode is preserved (25). To date, no unifying model regarding initiation of polymerization and subsequent fibril formation has been established; although, partial denaturation of TTR in an acidic environment and polymerization

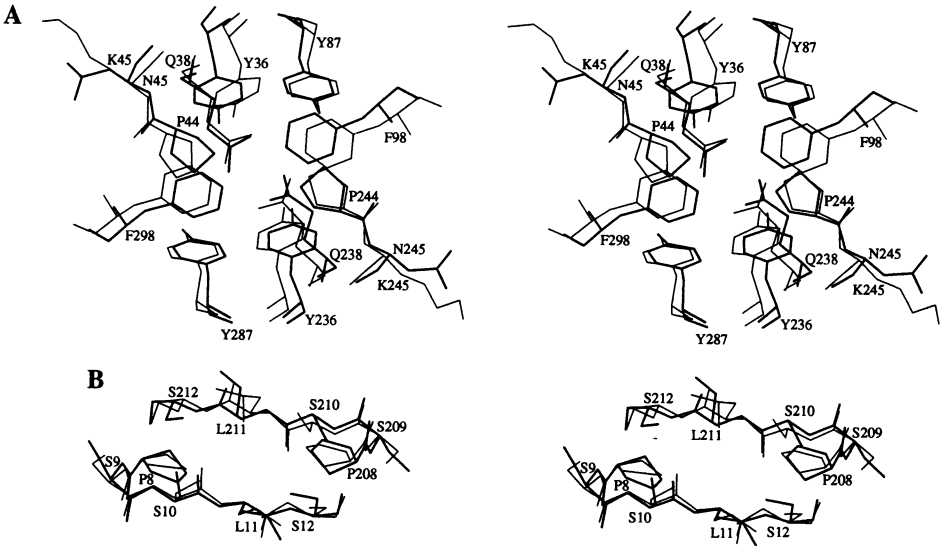

FIG. 5. (*A*) Stereo plot of BRE (thick lines) and REI (thin lines) structural comparison at V_L dimer interface. Displayed are contact-forming residues between monomers in light chain dimers. The second monomer has 200 added to its residue numbers. The local diad is perpendicular to the figure. (*B*) Stereo plot of BRE (thick lines) and REI (thin lines) structural comparison along dimer–dimer contact region. Displayed are contact-forming residues from adjacent monomers of dimer 1 and dimer 2. The second monomer has 200 added to its residue numbers. The local diad is perpendicular to the figure. The two figures were prepared with MOLSCRIPT (21) on the basis of least-squares superimposition of both coordinate sets (REI coordinate set: Protein Data Bank entry "1REI") and calculated and displayed with O (15). Labels indicate residue type (one-letter amino acid code) and number in the sequence.

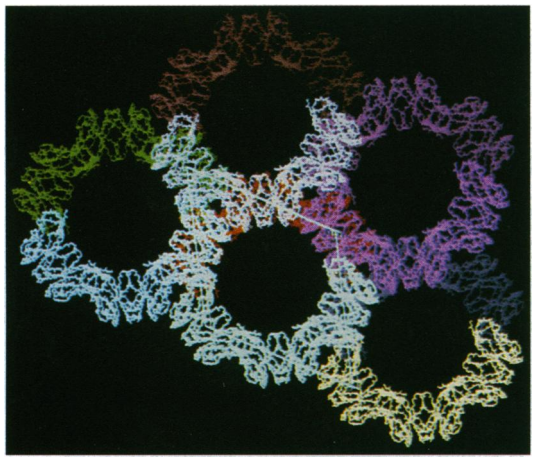

FIG. 6. Packing diagram of BRE crystal form I when viewed down the *b* axis (*y* direction). The *a* and *c* axes of the unit cell for BRE I are indicated by solid lines. Only backbone atoms are displayed.

via the cysteine residue (TTR residue 10) have been suggested as factors in this process (26, 27). The fibril model presented here for an amyloid-associated κ light chain shows a change in packing mode when compared with nonamyloid light chain proteins such as REI and ROY and is consistent with dimensions of amyloid fibrils determined by electron microscopy. While REI shows a regular hexagonal spiral structure (28), because of its unique primary structure it may be predisposed to form crystals *in vivo* rather than fibrils. This may be a basis for "myeloma kidney" seen in individuals with large amounts of Bence Jones proteins which do not form amyloid fibrils. We believe that the pseudohexagonal packing arrangement is not an artifact of crystal forces but a direct result of positional changes seen in our model, especially in the contact regions, and that this perturbation makes BRE more susceptible to amyloid fibril formation *in vivo*. The dimer–dimer contact region is probably more important in the aggregation process of light chain dimers than the dimer interface.

The model presented here can be tested by studying the tertiary structure of other amyloidogenic immunoglobulin light chain proteins of both subtypes (κ and λ). If this model holds, it may then be possible to identify key residues responsible for the transformation.

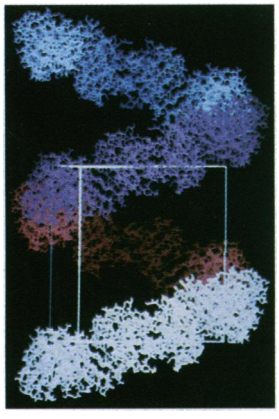

FIG. 7. Spiral model along *b* axis (*y* direction) based on pseudohexagonal structure of BRE I. There are six light chain dimers per turn of 360° along the *b* axis (*y* direction). Solid lines indicate the unit-cell dimensions.

We thank Dr. Marianne Schiffer for helpful discussions and encouragement in the early phases of these studies. This work was supported by Veterans Affairs Medical Research (MRIS 583-0888), and from U.S. Public Health Service Grants RR00750, DK34881, DK42111, AG10608, AR20582, the Arthritis Foundation, and the Marion E. Jacobson Fund.

1. Kyle, R. A. & Gertz, M. A. (1990) *Crit. Rev. Oncol. Hematol.* **10,** 49–87.
2. Glenner, G. G., Terry, W., Harada, M., Isersky, C. & Page, D. (1971) *Science* **172,** 1150–1151.
3. Solomon, A., Frangione, B. & Franklin, E. C. (1982) *J. Clin. Invest.* **70,** 453–460.
4. Dwulet, F. E., Strako, K. & Benson, M. D. (1985) *Scand. J. Immunol.* **22,** 653–660.
5. Liepnieks, J. J., Benson, M. D. & Dwulet, F. E. (1990) in *Amyloid and Amyloidosis*, ed. Natvig, J. B. (Kluwer, Dordrecht, The Netherlands), pp. 153–156.
6. Madisen, L., Hoar, D. I., Holroyd, C. D., Crisp, M. & Hodes, M. D. (1987) *Am. J. Med. Genet.* **27,** 379–390.
7. Kabat, E. A., Wu, T. T., Perry, H. M., Gottesman, K. S. & Foeller, C. (1991) *Sequences of Proteins of Immunological Interest* (National Institutes of Health, Bethesda), 5th Ed., pp. 1–4, 103–112.
8. Murrell, J. R., Schoner, R. G., Liepnieks, J. J., Rosen, H. N., Moses, A. C. & Benson, M. D. (1992) *J. Biol. Chem.* **267,** 16595–16600.
9. Colman, P. M., Schramm, H. J. & Guss, J. M. (1977) *J. Mol. Biol.* **116,** 73–79.
10. Sato, M., Yamamoto, M., Imada, K., Katsube, Y., Tanaka, N. & Higashi, T. (1992) *J. Appl. Crystallogr.* **25,** 348–357.
11. Brünger, A. T. (1990) *Acta Crystallogr. A* **46,** 46–57.
12. Brünger, A. T., Kuriyan, J. & Karplus, M. (1987) *Science* **235,** 458–460.
13. Epp, O., Lattman, E. E., Schiffer, M., Huber, R. & Palm, W. (1975) *Biochemistry* **14,** 4943–4952.
14. Brünger, A. T. (1991) *Annu. Rev. Phys. Chem.* **42,** 197–223.
15. Jones, T. A., Zou, J. Y., Cowan, S. W. & Kjeldgaard, M. (1991) *Acta Crystallogr. A* **47,** 110–119.
16. Bailey, S. (1994) *Acta Crystallogr. D* **50,** 760–763.
17. Brünger, A. T. (1992) *Nature (London)* **355,** 472–474.
18. Hendrickson, W. A. & Konnert, J. H. (1980) in *Biomolecular Structure, Function, Conformation and Evolution*, ed. Srinivisan, R. (Pergamon, Oxford), Vol. 1, pp. 43–57.
19. Read, R. J. (1986) *Acta Crystallogr. A* **42,** 140–149.
20. Eulitz, M. & Linke, R. P. (1982) *Hoppe Seyler's Z. Physiol. Chem.* **363,** 1347–1358.
21. Kraulis, P. J. (1991) *J. Appl. Crystallogr.* **24,** 946–950.
22. Bacon, D. J. & Anderson, W. F. (1988) *J. Mol. Graphics* **6,** 219–220.
23. Merritt, E. A. & Murphy, M. E. P. (1994) *Acta Crystallogr. D* **50,** 869–873.
24. Kabsch, W. & Sander, C. (1983) *Biopolymers* **22,** 2577–2637.
25. Hamilton, J. A., Steinrauf, L. K., Braden, B. C., Liepnieks, J. J., Benson, M. D., Holmgren, G., Sandgren, O. & Sten, L. (1993) *J. Biol. Chem.* **268,** 2416–2424.
26. Colon, W. & Kelly, J. W. (1992) *Biochemistry* **31,** 8654–8660.
27. Terry, C. J., Damas, A. M., Oliveira, P., Saraiva, M. J. M., Sakaki, Y. & Blake, C. C. F. (1993) *EMBO J.* **12,** 735–741.
28. Huang, D.-B., Chang, C.-H., Ainsworth, C., Brünger, A. T., Eulitz, M., Solomon, A., Stevens, F. J. & Schiffer, M. (1994) *Biochemistry* **33,** 14848–14857.